93093

Application of QFT to the Problem of Failed In-Flight Controllers During Approach and Landing of a B-720 Aircraft

Hwei-Lan Chou
Daniel J. Biezad

Cal Poly State University
San Luis Obispo, CA 93407

Abstract

Previous studies by NASA Dryden have shown the use of throttles for emergency flight control to be extremely difficult, especially for landing. Flight control using only the throttles to achieve safe landing for a large jet transport airplane, the Boeing 720, is investigated using Quantitative Feedback Theory. Results are compared to an augmented control developed in a previous study. The controller corrected unsatisfactory open-loop characteristics by increasing system bandwidth and damping, but improving the control bandwidth substantially proved very difficult. The pitch controller is robust in conditions of no or moderate turbulence. The roll controller performed well in conditions of no turbulence, but is sensitive to moderate turbulence. Handling qualities of the augmented control for approach and landing were evaluated by piloted simulation flights.

Notation

TOFC	Throttle-Only Flight Control
QFT	Quantitative Feedback Theory
C_{mu}	Velocity-pitch rate derivative
$C_{l\beta}$	Sideslip-roll coupling derivative
q	pitch rate (deg/sec)
γ	flight path angle (deg)
β	angle of sideslip (deg)
φ	bank angle (deg)
θ	pitch angle (deg)
z	thrust (lbs)
ω_1	natural frequency
ζ	damping ratio
δ_{Tc}	stick input(full deflection=1 unit)
K_q	pitch rate feedback gain
K_γ	flight path angle feedback gain
K_β	sideslip angle feedback gain
K_φ	bank angle feedback gain
G_{in}^{out}	transfer functions
(a)	short form of (s+a)
$\{\zeta,\omega\}$	short form for $s^2 + 2\zeta\omega s + \omega^2$
c.g.	center of gravity

Introduction

Through throttle manipulations, engine thrust has been found useful in providing some controllability for multiengine aircraft in emergency situations with severe or complete flight control system failures. This paper focuses on a particular application, a simulation augmented control developed by NASA for Boeing-720 aircraft Throttles-Only Flight Control (TOFC) [1-2]. NASA has found the use of throttles feasible for emergency flight control for a range of airplanes, and their analyses for a variety of aircraft are available in the literature [3-6]. This controller was implemented on a high fidelity B720 flight simulator and obtained generally good pilot ratings by increasing the bare airframe Dutch-roll and phugoid damping. The primary aim of this study is to present an alternative control design technique based on Quantitative Feedback Theory(QFT) to further improve the Dutch-roll damping and to increase controller bandwidth for better handling qualities.

The QFT technique [7] was chosen because of the insights it provides throughout its design process. It allows designers to specify a desired closed-loop frequency response with a desired control bandwidth and damping characteristic. It shows why the desired performance may not be achieved within the given control actuation and rate limits.

In this paper a QFT augmented throttle-only flight path controller for approach and landing is presented. Complete details of the aircraft model and justification for TOFC are not included, but the reader is reminded that "trimming" must be possible and "controllability" must exist. Augmented control design using QFT is presented in a summary fashion. The full justification and step by step procedure may be found in Reference 8.

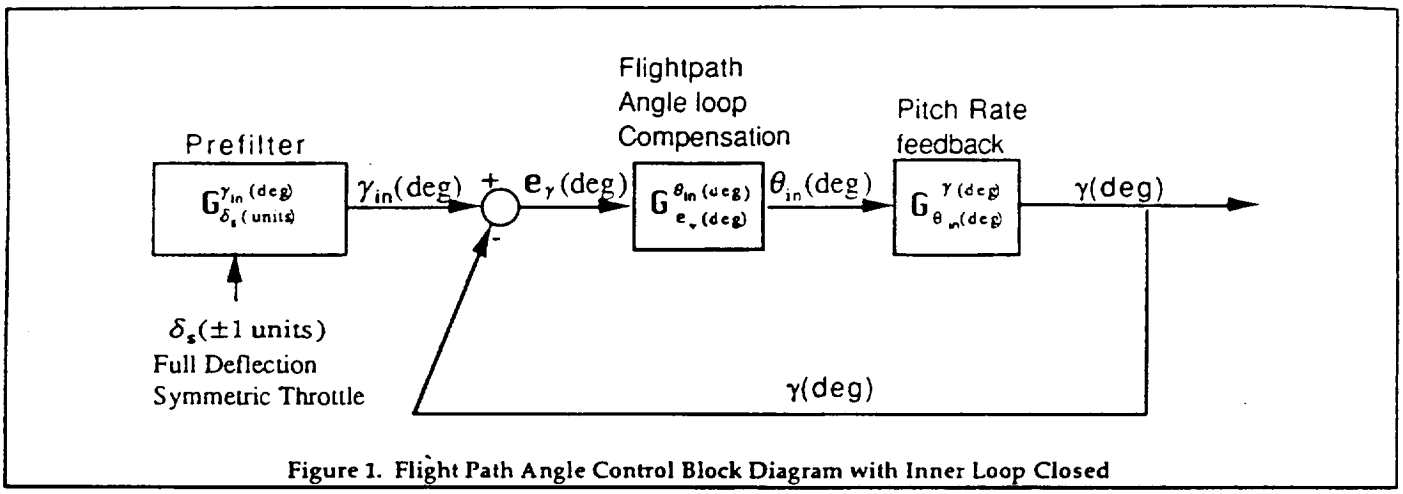

Figure 1. Flight Path Angle Control Block Diagram with Inner Loop Closed

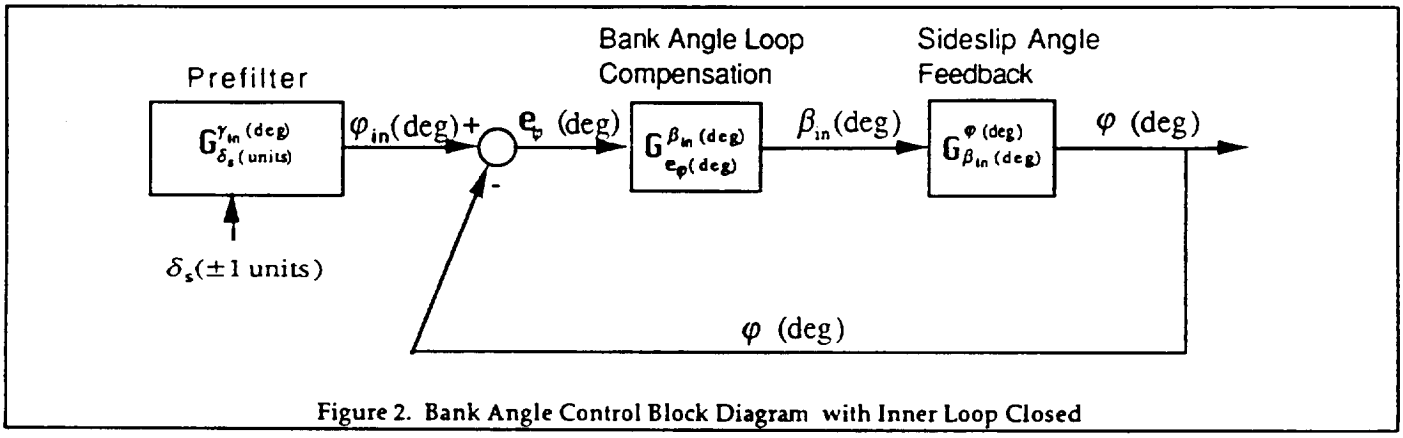

Figure 2. Bank Angle Control Block Diagram with Inner Loop Closed

B-720 Linear Model

The empirical transfer function developed for the engines is given in short form notation by

$$G^{z(lbs)}_{\delta_{th(s)}} = \frac{275}{(.55)(5)}$$

Severe bandwidth attenuation occurs beyond frequencies of 1 rad/sec. For this application his prevented the increase the closed-loop bandwidth beyond 1 rad/sec within the range of available thrust (see Ref. 6).

Four configuration variations for the B-720 were considered as described in the Appendix. They are characterized in both the longitudinal and lateral axes by excessive resonance, low phase and gain margins, low crossover frequency, and large phase angle roll-off.

QFT Controller Design

To apply QFT, the aircraft model is rearranged in a unit feedback form as shown in Figures 1 and 2. The inner pitch rate and sideslip loops were closed using Kq=60 and $K\beta = 4$, which were the settings for the original simulation augmentation scheme.

Performance Specification

QFT allows designers to specify a desired closed-loop frequency response with an upper bound B_U, a lower bound B_L, and a tolerance δ_R specified to obtain robust performance. The maximum M_m is also given to obtain a desired system damping.

Table 1. QFT Performance Specification

Freq.(r/s)	0.1	0.3	0.5	0.7	1.0	2.0	5.0
Bu(dB)	17.0	17.0	17.3	-16.0	-4.0	20	-13.0
BL(dB)	16.8	-15.0	12.3	4.6	-12.4	7.1	-23.0
δ_R (dB)	0.2	2	5	8.4	8.4	9.1	15.0

The performance specification shown in Table 1 are the desired closed-loop responses for both the γ - and φ - loops. These two feedback loops are piloted open-loop systems. Additional specifications are ususallly given for piloted systems, such as a desired control bandwidth of 2 rad/sec. (see Ref. 9 for transport aircraft landing requirements) and a k/s slope near the crossover frequency. These added requirements promote good pilot handling qualities.[10]

Design Constraints

Four configurations were used to study the approach and landing of B-720 throttle-only flight control as summarized in Table 2 and in the Appendix. Configuration 1 was used as the nominal confiuration for control design.

Table 2. Flight Configurations for B-720 (Gear Up)

Conf	Weight (lbs)	Alt (Ft) (MSL)	A/S (Kts)	Flaps (%)
1	140,000	4,000	160	0
2	140,000	4,000	145	30
3	160,000	4,000	175	0
4	140,000	4,000	155	30

The performance bounds constraint is a curve on the Nichols Chart that shows the performance tolerance, δ_R, from Table 1 at each specified frequency. Satisfying the tolerance constraint guarantees that the variation of the system response due to plant uncertainties will be no greater than δ_R. There is a performance bound for each frequency.

U contours are also shown on the Nichols Chart. The U contour is a M-circle that has the magnitude of M_m, with part of the circle stretched for uncertainty at high frequencies. By having the open-loop frequency response not penetrate the U contour, the system's damping will be guaranteed no less than the damping selected for M_m as a design constraint.

For inner-loop transfer functions $G^{\gamma}_{\theta_{in}}$ and $G^{\phi}_{\beta_{in}}$, the parameter variation given by the four configurations can be expressed minimums and maximums. There are tradeoffs between plant parameter variations and performance. The wider the parameter variation, the more restricted the constraints; consequently, more compensation is required. In this application, due to the engine response limits, the performance specification will have to be relaxed because there is not enough control power to provide all the compensation that is required to meet specifications.

The minimum and maximum values of transfer functions, $G^{\gamma}_{\theta_{in}}$ and $G^{\phi}_{\beta_{in}}$, form the uncertainty template. The QFT control package [11] allows the designer to input maximum and minimum plant parameter variations, but due to the software's limitation of handling the quantity of uncertainties, some of them were averaged. These variations are listed in Figures 3 and 4.

The $G^{\gamma(deg)}_{\theta_{in}(deg)}$ of the nominal configuration(config. 1) is:

$$G^{\gamma(deg)}_{\theta_{in}(deg)}\ \text{config. 1} = \frac{.01(.203)[.37,\ 3.01]}{(.562)\,[.624,\ .111]\,[.441,\ 1.57]\,(5.25)}$$

and the min. and max. $G^{\gamma(deg)}_{\theta_{in}(deg)}$ are:

$$G^{\gamma(deg)}_{\theta_{in}(deg)}\ \text{min.} = \frac{.0053\ (.162)\ [.35\ ,\ 3.01]}{(.40)\,[.42\ ,\ 1.48]\,[.66\ ,\ .01]\,(5.19)}$$

$$G^{\gamma(deg)}_{\theta_{in}(deg)}\ \text{max.} = \frac{.01\ \ (.28)\ [.46,\ 3.43]}{(.58)\,[.45\ ,\ 1.57]\,[.92\ ,\ .14]\,(5.24)}$$

Figure 3. Longitudinal Mode Parameter Variation

The $G^{\phi(deg)}_{\beta_{in}(deg)}$ of the nominal configuration(config. 1) is:

$$G^{\phi(deg)}_{\beta_{in}(deg)}\ \text{nominal} = \frac{.09\ [.47\ ,\ 3.65]}{(.98)\,[.81\ ,\ .15]\,[.26\ ,\ 1.07]\,(5.02)}$$

and the min. and max. of $G^{\phi(deg)}_{\beta_{in}(deg)}$ are:

$$G^{\phi(deg)}_{\beta_{in}(deg)}\ \text{min.} = \frac{.06\ [.45\ ,\ 3.65]}{(.98)\,[.60\ ,\ .15]\,[.24\ ,\ .93]\,(5.01)}$$

$$G^{\phi(deg)}_{\beta_{in}(deg)}\ \text{max.} = \frac{.09\ [.61\ ,\ 4.33]}{(1.03)\,[1.0\ ,\ .20]\,[.29\ ,\ 1.09]\,(5.02)}$$

Figure 4 Lateral Mode Parameter Variation

Controller Design Technique

Poles/zeros/gain compensation will be required to reshape the open- loop transfer functions from $G^{\gamma}_{\theta_{in}}$ and $G^{\phi}_{\beta_{in}}$. On the Nichols Chart, gain raises the transfer function curve, a zero bends the curve to the right, and a pole bends the curve to the left. The compensation-selected forms the controller, G_c. $G^{\gamma}_{\theta_{in}}$ and $G^{\phi}_{\beta_{in}}$ after reshaping, become respectively $L^{\gamma}_{e\gamma}$ and $L^{\phi}_{e\phi}$, the open-loop transfer functions of the flight path angle and bank angle feedback loops, where $L^{\gamma}_{e\gamma} = G^{\theta_{in}}_{e\gamma} * G^{\gamma}_{\theta_{in}}$ and $L^{\phi}_{e\phi} = G^{\beta_{in}}_{e\phi} * G^{\phi}_{\beta_{in}}$. $L^{\gamma}_{e\gamma}$ and $L^{\phi}_{e\phi}$ should be kept on and above the Bo($j\omega_i$), for each frequency, ω_i, on $L^{\gamma}_{e\gamma}$ and $L^{\phi}_{e\phi}$ to assure robust performance. $L^{\gamma}_{e\gamma}$ and $L^{\phi}_{e\phi}$ must also not penetrate the U contour in order to obtain the desired damping. In this application the additional constraint existed which required the controller to be physically realizable (zeros not outnumbering poles).

Longitudinal Flight Path Angle Controller

Transfer function $G^{\gamma}_{\theta_{in}}$ and its performance bounds, Bo($j\omega_i$), and U contour are displayed on a Nichols Chart in Figure 5. Since all the frequency points for $G^{\gamma}_{\theta_{in}}$ are below their corresponding Bo($j\omega_i$).reshaping is required. Pure gain compensation first raises the curve until it touches the U contour as shown in Figure 6($G^{\theta_{in}}_{\gamma}$ =16). Compensation is then added to avoid the U contour while satisfying all the Bo($j\omega_i$) constraints. Note that no realizable poles/zero compensation could be found to do this. A zero at .1 rad/sec, for example, pulls the whole $G^{\gamma}_{\theta_{in}}$ curve to the right of the U contour. But then a pole at any location would make the $G^{\gamma}_{\theta_{in}}$ curve penetrate the U contour. Since a compensator with only one zero is physically ununrealizable for this application, the compensator, G_c, for the flight path angle feedback loop, $G^{\theta_{in}}_{e_\gamma}$, is a pure gain of 16. The performance bound, hence the system robustness, was left unsatisfied.

The frequency response of the close-loop transfer function, $T^{\gamma}_{\gamma_{in}}$, where

$$T^{\gamma}_{\gamma_{in}} = L^{\gamma}_{e\gamma} / (1 + L^{\gamma}_{e\gamma}) = (G^{\theta_{in}}_{e\gamma} * G^{\gamma}_{\theta_{in}}) / (1 + G^{\theta_{in}}_{e\gamma} * G^{\gamma}_{\theta_{in}})$$

is shown in Figure 7. It can be seen in Figure 7 that δ_T, the spread between T_{max} and T_{min}, has exceeded the δ_B over the frequency range .1 to .7 rad/sec. This is because $L^{\gamma}_{e\gamma}$ did not satisfy the performance bounds over that frequency range. The frequency plot of the close-loop response after adding a prefilter is shown in Figure 8. A pure gain prefilter of 6 proved most effective in increasing the bandwidth and in meeting the prescribed specification.

Lateral Bank Angle Controller

Transfer function $G^{\phi}_{\beta_{in}}$ and its performance bounds, Bo($j\omega_i$), and U contour were similarly analyzed on a Nichols Chart. $G^{\phi}_{\beta_{in}}$ was not only below all the Bo($j\omega_i$) but also penetrated the U contour. A controller, $G^{\beta_{in}}_{e\phi}$ =(s+.15)/(s+1.5), was added to $G^{\phi}_{\beta_{in}}$ to reshape it. $L^{\phi}_{e\phi}$ is shown on a Nichols Chart in Figure 9 and t... frequency plot of the close-loop transfer function, $T^{\phi}_{\phi_{in}}$, where $T^{\phi}_{\phi_{in}} = L^{\phi}_{e\phi} / (1 + L^{\phi}_{e\phi}) = (G^{\beta_{in}}_{e\phi} * G^{\phi}_{\beta_{in}}) / (G^{\beta_{in}}_{e\phi} * G^{\phi}_{\beta_{in}})$, is shown in Figure 10 which shows the close-loop frequency response of $T^{\phi}_{\phi_{in}}$ after reshaping but with no prefilter applied yet. Sufficient gain is available here. A lead compensator of (S+1)/(S+2) is added to haunch up the severely deteriorated curve at frequencies over 1 rad/sec, and a lag compensator of (S+.25)/(S+.15) is added to steeper the gain curve at low frequencies to provide a smoother k/s curve for good pilot handling qualities. The close-loop response after adding the prefilter is similar to Figure 8, The prefilter selected is 15(S+.25)(S+1)/((S+.15)(S+2)).

Results and Discussion

For bank angle control using only the throttles, β feedback was found effective in increasing Dutch-roll damping. Bank angle feedback is crucial to lateral phugoid damping. Yaw rate feedback, on the other hand, increases Dutch-roll damping very little and actually decreases the lateral phugoid damping. Tables 4 and 5 compare the dynamic modes of the bare airframe with those from the augmented control implemented in a previous simulation study (References 1 and 2), and with those from the QFT implementation.

Table 3. Longitudinal Mode Comparison

	Density	Phugoid	Short Period	Engine	Pre-Filter	$G^{\theta_{in}}_{e_\gamma}$	$G^{\delta_{T_c}}_{e_\theta}$	K_γ	K_q
Bare Airframe	(1.4E-6)	(.04,.13)	(.65,1.4)	(.55)(5.2)	*	*	*	*	*
Simulation Augmented Control	(4.7E-6)	(.52,.24)	(.52,1.5)	(.4)(5.2)	10	1	10	1	4
QFT Augmented Control	(3.4E-6)	(.62,.32)	(.46,1.6)	(.3)(5.2)	6	16	1	1	60

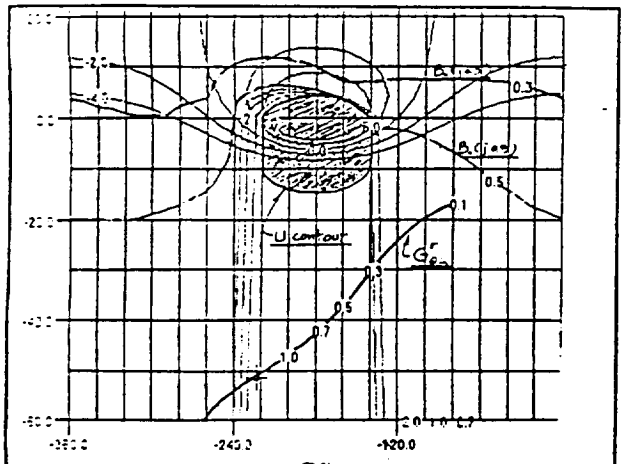

Figure 5.Transfer function $G^{\gamma}_{\theta_{in}}$, its performance bounds B(jw), and U contour on Nichols Chart

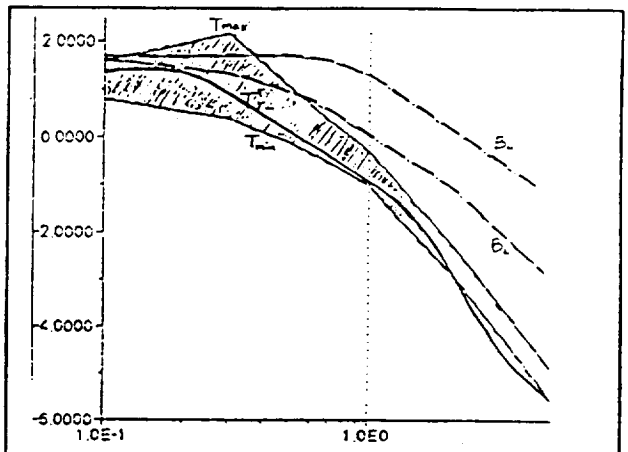

Figure 8. Frequency plot of the close-loop transfer function $T^{\gamma}_{\gamma_{in}}$ with prefilter

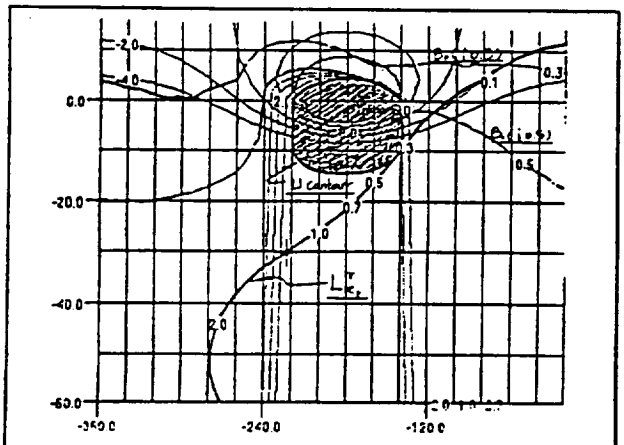

Figure 6. Open-loop transfer function, $L^{\gamma}_{\theta_{in}}$

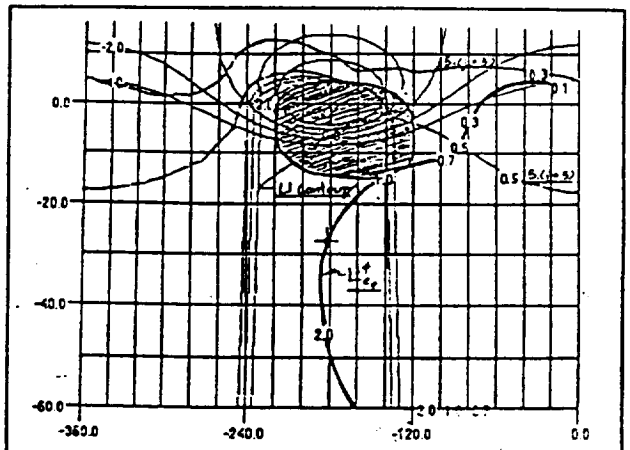

Figure 9. Open-loop transfer function, $L^{\varphi}_{e\varphi}$, on Nichols Chart

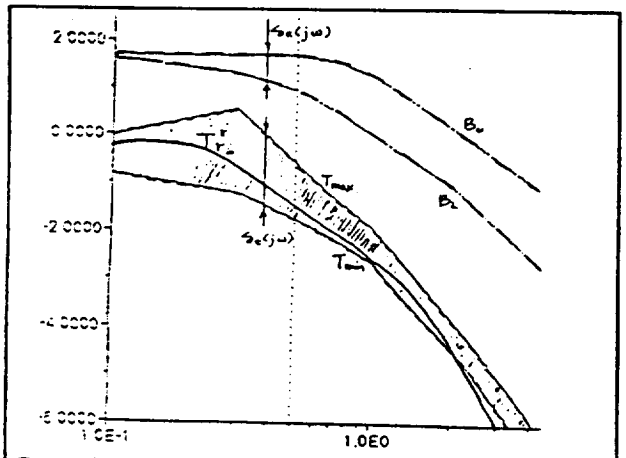

Figure 7. Frequency plot of the close-loop transfer function $T^{\gamma}_{\gamma_{in}}$ with no prefilter

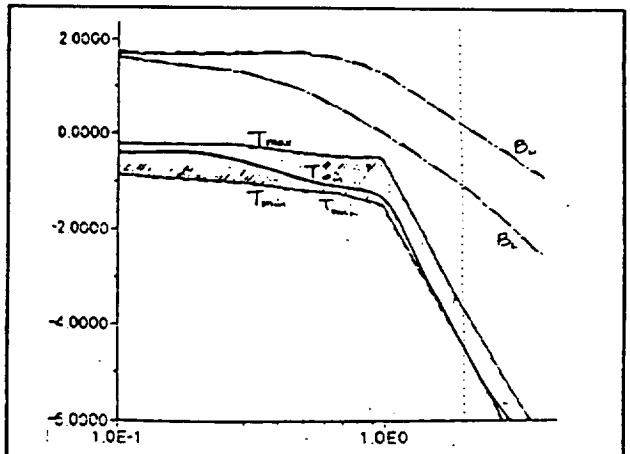

Figure 10. Frequency plot of the close-loop transfer function $T^{\varphi}_{\varphi_{in}}$ with no prefilter

Table 4 Lateral Mode Comparison

	Spiral	Dutch Roll	Roll	Engine	Pre-Filter	$G_{e_\phi}^{\beta_\phi}$	$G_{e_\phi}^{\delta_{r_c}}$	K_ϕ	K_β	K_p
Bare Airframe	(1.1E-4)	(.12,.99)	(1)	(.55)(5)	*	*	*	*	*	*
Simulation Augmented Control	(.73,.35)	(.15,.99)	(1)	(5)	40	1	1	.5	1	.5
QFT Augmented Control	(.39)	(.29,1.0)	(1.5)	(.45)(5)	$\frac{2.5(.25)}{(1.25)}$	1	1	$\frac{(.15)}{(1.5)}$	4	*

For longitudinal control, pure gain compensation was used. The short period mode has a frequency near 1.5 rad/sec, which is beyond the frequency that the throttles can control. Therefore, the primary concern was to increase phugoid damping and frequency. The short period damping decreased from .52 to .46 rad/sec while the phugoid damping and frequency increased from .52 to .62 and from .24 rad/sec to .32 rad/sec, respectively. This increase of response frequency can also be easily seen on the flight path angle response (not shown here).

For lateral control where pole/zero compensation was used, the Dutch-roll damping was almost doubled, from .15 to .29. The "simulation augmented controller" caused a lateral phugoid mode, [.73, .35], which combines the spiral and the slow engine mode. The QFT controller eliminated the lateral phugoid mode and resulted in higher damping for the Dutch roll mode (0.29 versus 0.15).

Turbulence Response

The response of the QFT flight path controller under intermediate turbulence was excellent. Since gusts were input, more than one simulation run was made to examine the tracking integrity under turbulence. Both controllers performed well, but the lateral QFT controller showed undue sensitivity to $K\beta$ during bank angle tracking.

During investigation of the bank angle tracking problem, it was found that the β being feedback in the simulation was the β at the c.g. instead of at the nose boom. The nose boom β was then modeled into the B-720 simulator, which improved the bank angle tracking under turbulence. The β at the nose boom has two extra terms, one a function of roll rate, the other a function of yaw rate. It was thought that the extra yaw rate term might have stabilized the bank angle tracking (the roll rate term was too small and was neglected.)

System response to configuration variations, for flight path control and for bank angle control, was very good. The robustness of the flight path control was improved by QFT. The Dutch-roll oscillation in the original simulation compensation was taken out by QFT compensation; however, the tracking did not improve.

Conclusions and Recommendations

For throttles-only pitch control using a QFT controller, the control bandwidth , tracking and control robustness were improved by QFT. For bank angle control, QFT has improved the Dutch-roll oscillation problem and performed well under no turbulence. However, the lateral phugoid tracking under intermediate turbulence did not perform well. Apparently a compromise is required between Dutch-roll and lateral phugoid mode damping. Further investigation is recommended for bank angle tracking under turbulence. The impact of system non-linearities, such as rate and thrust limits, was significant and resulted in a decrease in the bandwidth specification used in the QFT analysis.

Acknowledgment

This work was made possible by NASA Grant NCC 2-711. Thanks also goes to Mr. Glen Gilyard , Mr. Bill Burcham , and Jeanette Le at NASA Dryden for their technical support and guidance.

References

1. Burcham, F., Fullerton G., Gilyard, G., Conley, J. and J. Stewart, "A Preliminary Investigation of the Use of Throttles for Emergency Flight Control," NASA T.M. 4320, 1991.

2. Gilyard, G.B., Conley, J.L., Le, J., and F.W. Burcham, "A Simulation Evaluation of a Four-Engine Jet Transport Using Engine Thrust Modulation for Flight Path Control," AIAA-91-2223, 27th Joint Propulsion Conference, June 24-26, 1991, Sacramento, CA.

3. Azzano, C.P., "A Preliminary Look at Optimal Multi-Variable Design of Propulsion-Only Flight Controllers for Jet Transport Aircraft," NASA Dryden TR, Sept 21, 1990.

4. Biezad, D.J., "The Propulsive-Only Flight Control Problem," NAECON , Vol 2, pp494-500, Dayton, Ohio, May 20-24, 1991.

5. Biezad, D.J. and C.P. Azzano, "Designing Low Bandwidth Propulsive-Only Flight Controllers", AIAA Guidance, Navigation, and Control Conference, Paper #91-2628CP, pp 267-275, August 12-14, 1991, New Orleans, La.

6. Chou, Hwei-Lan and D.J. Biezad, "Pilot-in-the-Loop Analysis of Propulsive-Only Flight Control Systems," National Aerospace Electronics Conference, Vol. 2, pp 482-488, Dayton, Ohio, May 1822, 1992.

7. Horowitz,I. M. ,and Sidi,M., "Synthesis of feedback systems with large plant ignorance for prescribed time-domain tolerances" Int. J. Control, Vol.16, pp.287-309, 1972.

8. Chou, H.L., "Low Bandwidth Robust Controllers for Flight," Master's Thesis, Cal Poly State University, 1993.

9. Sarrafian, S.K., and Powers, B.G., "Application of Frequency Domain Handling Qualiities Criteria to the Longitudinal Landing Task." NASA Technical Memorandum, Aug. 1985.

10 MIL-STD-1797A, "Flying Qualities of Piloted Vehicles", limited distribution, ASD/ENES, Wright-Patterson AFB, Ohio, 30 Jan 1990.

11. Yaniv, O., "Multiple-input single-output (MISO) User Manual, Tel-Aviv University, 1991.

Appendix

Longitudinal Transfer Functions:

$$G^{q(\text{deg/sec})}_{z(\text{lbs})} = N^{q(\text{deg/sec})}_{z(\text{lbs})} / \Delta_{long}$$

$$G^{\gamma(\text{deg})}_{z(\text{lbs})} = N^{\gamma(\text{deg})}_{z(\text{lbs})} / \Delta_{long}$$

$$N^{q(\text{deg/sec})}_{z(\text{lbs})} = \begin{bmatrix} 2.36E-04 & (0) & (-1.17E-05) & (0.370, & 0.61) \\ 2.33E-04 & (0) & (1.4E-06) & (0.635, & 0.563) \\ 1.976E-04 & (0) & (0.292) & (0.644) & \\ 1.955E-04 & (0) & (2.68E-06) & (0.819, & 0.508) \end{bmatrix}$$

$$N^{\gamma(\text{deg})}_{z(\text{lbs})} = \begin{bmatrix} 2.796E-05 & (0) & (0.203) & (0.370, & 3.008) \\ -1.819E-05 & (0) & (0.364) & (2.255) & (-4.452) \\ 2.130E-05 & (0.167) & (0.351, & 3.038) & \\ 1.470E-05 & (0) & (0.261) & (0.460, & 3.426) \end{bmatrix}$$

$$\Delta_{long} = \begin{bmatrix} (1.438E-05) & (3.918E-02, & 0.130) & (0.652, & 1.382) \\ (1.101E-05) & (7.423E-02, & 0.147) & (0.596, & 1.375) \\ (3.949E-02, & 0.118) & (0.649, & 1.301) & \\ (1.878E-05) & (7.190E-02, & 0.138) & (0.588, & 1.279) \end{bmatrix}$$

Lateral Transfer Functions:

$$G^{\beta(\text{deg})}_{z(\text{lbs})} = N^{\beta(\text{deg})}_{z(\text{lbs})} / \Delta_{lat}$$

$$G^{\phi(\text{deg})}_{z(\text{lbs})} = N^{\phi(\text{deg})}_{z(\text{lbs})} / \Delta_{lat}$$

$$N^{\beta(\text{deg})}_{z(\text{lbs})} = \begin{bmatrix} -1.58E-03 & (-.0805) & (.927) \\ -1.59E-03 & (-.0922) & (.904) \\ -1.43E-03 & (-.0723) & (.981) \\ -1.44E-03 & (-.0879) & (.940) \end{bmatrix}$$

$$N^{\phi(\text{deg})}_{z(\text{lbs})} = \begin{bmatrix} 3.19E-04 & (.468, & 3.65) \\ 2.15E-04 & (.611, & 4.17) \\ 2.89E-04 & (.447, & 3.96) \\ 2.04E-04 & (.593, & 4.33) \end{bmatrix}$$

$$\Delta_{lat} = \begin{bmatrix} (.0001) & (1.01) & (.116, & 1.05) \\ (.006) & (1.05) & (.067, & 0.93) \\ (.0028) & (1.06) & (.114, & 1.08) \\ (.0065) & (1.09) & (.060, & .944) \end{bmatrix}$$